ACCOUNTS of chemical research

Article

pubs.acs.org/accounts

Identification of Atomic-Level Mechanisms for Gas-Phase $X^- + CH_3Y$ S_N2 Reactions by Combined Experiments and Simulations

Jing Xie,[†] Rico Otto,[‡] Jochen Mikosch,[§] Jiaxu Zhang,[∥] Roland Wester,[⊥] and William L. Hase*[,†]

[†]Department of Chemistry and Biochemistry, Texas Tech University, Lubbock, Texas 79409, United States

[‡]Department of Chemistry and Biochemistry, University of California, San Diego, 9500 Gilman Drive, La Jolla, California 92093, United States

[§]Max-Born-Institute, Max-Born-Strasse 2A, D-12489 Berlin, Germany

[∥]Institute of Theoretical and Simulational Chemistry Academy of Fundamental and Interdisciplinary Sciences, Harbin Institute of Technology, Harbin 150080, P. R. China

[⊥]Institut für Ionenphysik and Angewandte Physik, Universität Innsbruck, Technikerstrasse 25/3, A-6020 Innsbruck, Austria

CONSPECTUS: For the traditional model of gas-phase $X^- + CH_3Y$ S_N2 reactions, C_{3v} ion-dipole pre- and postreaction complexes X^----CH_3Y and XCH_3---Y^-, separated by a central barrier, are formed. Statistical intramolecular dynamics are assumed for these complexes, so that their unimolecular rate constants are given by RRKM theory. Both previous simulations and experiments have shown that the dynamics of these complexes are not statistical and of interest is how these nonstatistical dynamics affect the S_N2 rate constant. This work also found there was a transition from an indirect, nonstatistical, complex forming mechanism, to a direct mechanism, as either the vibrational and/or relative translational energy of the reactants was increased. The current Account reviews recent collaborative studies involving molecular beam ion-imaging experiments and direct (on-the-fly) dynamics simulations of the S_N2 reactions for which Cl^-, F^-, and OH^- react with CH_3I. Also considered are reactions of the microsolvated anions $OH^-(H_2O)$ and $OH^-(H_2O)_2$ with CH_3I. These studies have provided a detailed understanding of the atomistic mechanisms for these S_N2 reactions.

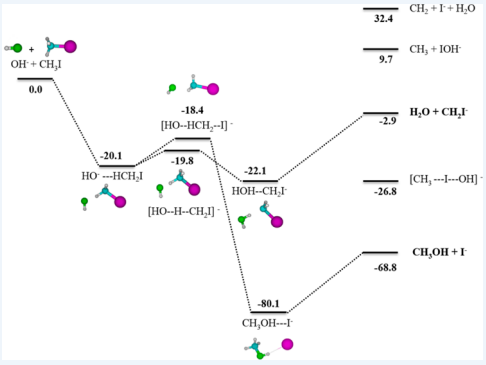

Overall, the atomistic dynamics for the $Cl^- + CH_3I$ S_N2 reaction follows those found in previous studies. The reaction is indirect, complex forming at low reactant collision energies, and then there is a transition to direct reaction between 0.2 and 0.4 eV. The direct reaction may occur by rebound mechanism, in which the $ClCH_3$ product rebounds backward from the I^- product or a stripping mechanism in which Cl^- strips CH_3 from the I atom and scatters in the forward direction. A similar indirect to direct mechanistic transition was observed in previous work for the $Cl^- + CH_3Cl$ and $Cl^- + CH_3Br$ S_N2 reactions. At the high collision energy of 1.9 eV, a new indirect mechanism, called the *roundabout*, was discovered.

For the $F^- + CH_3I$ reaction, there is not a transition from indirect to direct reaction as E_{rel} is increased. The indirect mechanism, with prereaction complex formation, is important at all the E_{rel} investigated, contributing up ~60% of the reaction. The remaining direct reaction occurs by the rebound and stripping mechanisms.

Though the potential energy curve for the $OH^- + CH_3I$ reaction is similar to that for $F^- + CH_3I$, the two reactions have different dynamics. They are akin, in that for both there is not a transition from an indirect to direct reaction. However, for $F^- + CH_3I$ indirect reaction dominates at all E_{rel}, but it is less important for $OH^- + CH_3I$ and becomes negligible as E_{rel} is increased. Stripping is a minor channel for $F^- + CH_3I$, but accounts for more than 60% of the $OH^- + CH_3I$ reaction at high E_{rel}.

Adding one or two H_2O molecules to OH^- alters the reaction dynamics from that for unsolvated OH^-. Adding one H_2O molecule enhances indirect reaction at low E_{rel}, and changes the reaction mechanism from primarily stripping to rebound at high E_{rel}. With two H_2O molecules the dynamics is indirect and isotropic at all collision energies.

I. INTRODUCTION

Nucleophilic substitution reactions are important in chemistry and biochemistry, and their early study was principally the province of physical organic chemistry. Pioneering work addressing mechanisms of these reactions was performed by Ingold[1] who established that primary alkyl halides underwent a bimolecular S_N2 reaction, for example, $X^- + CH_3Y \rightarrow XCH_3 + Y^-$. Both experiments[2] and electronic structure calculations[3] have shown these reactions are characterized by a potential energy curve with pre- and postreaction complexes, separated by a central barrier,[4−7] as illustrated in Figure 1.[8] For $Cl^- + CH_3I$ these complexes are ion-dipole Cl^----CH_3I and $ClCH_3$---I^- complexes with C_{3v} symmetry, the same symmetry as the central barrier.

Received: April 30, 2014
Published: August 14, 2014

   dx.doi.org/10.1021/ar5001764 | *Acc. Chem. Res.* 2014, 47, 2960−2969

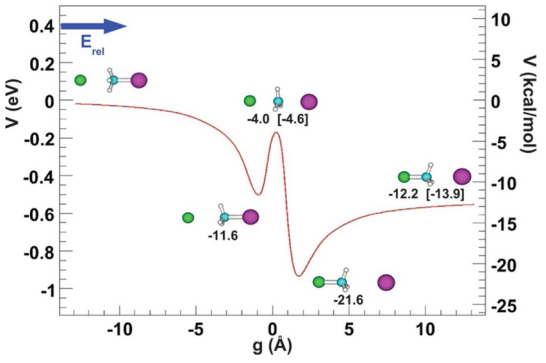

Figure 1. MP2(fc)/ECP/aug-cc-pVDZ potential energy curve for the Cl^- + CH_3I S_N2 reaction. Zero-point energies are not included. Experimental values are in brackets. Adapted with permission from ref 8. Copyright (2008) AAAS (The American Association for the Advancement of Science).

The first detailed atomistic model for the S_N2 reaction mechanism was proposed by Brauman and co-workers.[2,5] It assumes the reaction first forms the X^----CH_3Y prereaction complex, which can either cross the central barrier to form the postreaction complex XCH_3---Y^- or dissociate back to reactants. Similarly, the postreaction complex can dissociate to the XCH_3 + Y^- products or return to the prereaction complex. The mechanism is written as

$$X^- + CH_3Y \rightleftarrows X^-\text{---}CH_3Y \rightleftarrows XCH_3\text{---}Y^- \rightarrow XCH_3 + Y^- \quad (1)$$

Statistical dynamics, with rapid intramolecular vibrational energy redistribution, are assumed for both the pre- and postreaction complexes, so their unimolecular rate constants are given by RRKM theory.[9] Dependent on the height of the central barrier, the S_N2 rate constant has two limiting forms. If the central barrier is high and crossing the barrier is rate determining, the rate constant is that of transition state theory (TST) with the TS at the central barrier, and trapping in the prereaction complex is not required for the statistical model. On the other hand, if the central barrier is unimportant, the S_N2 rate constant is given by the rate of forming the prereaction complex. For the general case, the dissociation and crossing the central barrier unimolecular reactions of the prereaction complex are competitive and the S_N2 rate constant depends on the fraction of the prereaction complexes which cross the central barrier.[7]

Chemical dynamics simulations indicate that the above statistical model for the S_N2 reaction dynamics is incomplete.[7,10−12] This work found that the unimolecular dynamics of the X^----CH_3Y complex is nonstatistical, with weak coupling between the complex's low frequency intermolecular modes and higher frequency intramolecular modes,[7,11] and that a direct reaction without complex formation is promoted by exciting the C−Y stretching mode of the reactants.[7,10] Later experimental studies focused on the dynamics of the prereaction complex and confirmed the simulation predictions. Major findings of this experimental work is that the unimolecular decay of the X^----CH_3Y complex is nonexponential,[13] giving rise to a non-RRKM low-pressure unimolecular rate constant;[14,15] the unimolecular dynamics of the Cl^----CH_3Br complex is mode specific;[16] the statistical model does not represent the Cl^- + CH_3Br S_N2 rate constant versus either temperature,[17−19] reactant translational energy,[20,21] or CH_3Br vibrational and rotational energies;[20] and the $ClCH_3$ + Br^- product energy partitioning for the Cl^- + CH_3Br reaction is nonstatistical.[22,23]

Experiments have not investigated the simulation finding that a direct reaction is promoted by reactant C−Y vibrational excitation. However, experiments in concert with simulations indicate there is a transition from an indirect, prereaction complex forming mechanism to a direct mechanism without complex formation as the reactant collision energy E_{rel} is increased for the Cl^- + CH_3Cl[24,25] and Cl^- + CH_3Br[23,26] S_N2 reactions.

In recent research, combined molecular beam ion imaging experiments and chemical dynamics simulations have provided more complete and detailed "pictures" of the atomistic mechanisms of X^- + $CH_3Y \rightarrow XCH_3$ + Y^- S_N2 nucleophilic substitution reactions. The simulations are performed by direct dynamics in which the potential energy surface (PES) information required for the calculations is obtained directly from an electronic structure theory, without the need for an analytic potential energy function, that is, "on-the-fly" dynamics. The S_N2 reactions studied by these combined experiments and simulations are Cl^- + CH_3I,[8,27] F^- + CH_3I,[28,29] OH^- + CH_3I,[30−33] and $OH^-(H_2O)_n$ + CH_3I.[32−34] The reactions have both ion-dipole and hydrogen-bonded pre- and postreaction complexes, proceed via multiple indirect and direct mechanisms, and have important nonstatistical attributes in their reaction dynamics. As discussed previously,[7] the simulations are expected to give accurate results for these reactions. They are exothermic and zero-point energy effects are not important in assigning product energies. The direct reaction dynamics and the nonstatistical dynamics for the short-lived reaction intermediates are expected to be well-described by the simulations. It is noteworthy that the rate constants measured for the OH^- + CH_3I reaction[31] are accurately reproduced by the simulations. The results of the experimental and simulation studies are described here.

II. ATOMIC-LEVEL REACTION MECHANISMS

Experiments and simulations have identified multiple atomic-level direct and indirect mechanisms for X^- + $CH_3Y \rightarrow XCH_3$ + Y^- S_N2 nucleophilic substitution reactions, which are summarized in Table 1. The direct mechanism occurs by both rebound and stripping, and front side attack. There is CH_3 inversion for the former two. For rebound, the XCH_3 product rebounds off the Y atom, scattering in the backward direction. For stripping,[35] X^- strips CH_3 away from the Y atom with the XCH_3 product scattering in the forward direction. Frontside attack occurs without CH_3 inversion, with X^- directly displacing Y^-. There are

Table 1. Atomistic X^- + CH_3Y S_N2 Reaction Mechanisms

direct	*Rebound*: X^- attacks the backside of CH_3Y, directly displacing Y^-, and scattering in the backward direction with CH_3 inversion. Tends to be a small impact parameter event; refs 28 and 30.
	Stripping: X^- approaches the side of CH_3Y, stripping off CH_3, and scattering in the forward direction, with CH_3 inversion. Tends to be a large impact parameter event; refs 28, 30, and 35.
	Front side attack: X^- attacks the front-side of CH_3Y and directly replaces Y^- without CH_3 inversion; ref 30.
indirect	*Ion−dipole complex*: X^----CH_3Y and XCH_3---Y^- pre- and postreaction complexes; refs 2 and 5.
	Hydrogen-bonded complex: X^----HCH_2Y prereaction and CH_3X---Y^- (X = OH^-) postreaction complexes, refs 28 and 30
	Roundabout: X^- collides with CH_3Y and the CH_3 group rotates around Y one or more times before S_N2 substitution occurs; refs 8 and 30.
	Barrier recrossing: nonstatistical recrossing of the S_N2 $[X\text{--}CH_3\text{--}Y]^-$ central barrier; refs 7 and 12.

dx.doi.org/10.1021/ar5001764 | Acc. Chem. Res. 2014, 47, 2960−2969

numerous indirect mechanisms involving either formation of an ion-dipole and/or hydrogen-bonded prereaction complex, the postreaction complex, the roundabout mechanism, central barrier recrossings, or combinations of these mechanisms. Snapshots of the direct rebound and stripping mechanisms are depicted in Figure 3 of ref 28, and snapshots for the roundabout mechanism are depicted in Figure 3 of ref 8. Animations, providing atomistic details of these mechanisms, are given on the web portal hase-group.ttu.edu.

Mechanisms observed from simulations of the $Cl^- + CH_3I$, $F^- + CH_3I$, and $OH^- + CH_3I$ S_N2 reactions versus collision energy E_{rel}, and their relative importance, are summarized in Table 2. Also given are the averages f_{int} of the available product energy released to XCH_3 rovibrational internal energy, which are compared with experiment. In the following, detailed dynamics for these reactions are described.

Table 2. Atomistic Mechanisms and Product Energy Partitioning for S_N2 Reactions[a]

E_{rel} (eV)	rebound	stripping	indirect	f_{int}[b]
		$Cl^- + CH_3I$[8,27]		
0.20	0.17		0.83	0.86 ± 0.03
0.39	0.88	0.11	0.01	0.51 ± 0.04 (∼0.84)
0.76	1.00			0.46 ± 0.08 (∼0.40)
1.07	0.87		0.13	0.24 ± 0.01 (∼0.25)
1.90	0.73	0.09	0.18	0.38 ± 0.05 (∼0.40)
		$F^- + CH_3I$[28,29]		
0.32	0.15	0.25	0.60	0.69 ± 0.02 (∼0.70)
1.53	0.29	0.12	0.59	0.63 ± 0.04 (∼0.59)
		$OH^- + CH_3I$[30,33]		
0.05	0.33	0.28	0.39	0.80 ± 0.01
0.50	0.23	0.35	0.42	0.75 ± 0.02 (∼0.66)
1.00	0.18	0.63	0.19	0.76 ± 0.02 (∼0.71)
2.00[c]	0.30	0.64	0.03	0.68 ± 0.02 (∼0.71)

[a]The results are from direct dynamics simulations. Experimental results are in parentheses. [b]f_{int} is the fraction of the available energy partitioned to product rovibration. [c]At 2.00 eV, front side attack contributes 0.03 of the reaction mechanisms.

A. $Cl^- + CH_3I$ Reaction Dynamics

This reaction was studied experimentally at E_{rel} of 0.39, 0.76, 1.07, and 1.9 eV.[8] Center-of-mass images of the scattered I^- product are shown in Figure 2, along with the distribution of the energy transfer $Q = E_{kin,final} - E_{kin,initial}$ for the reactive events. These images show the directions the I^- products scatter after they are formed by the $Cl^- + CH_3I$ collisions. The translational energy of the scattered I^- product increases as its image moves from the center. There are extensive changes in the scattering dynamics as E_{rel} is increased. At 0.39 eV, the scattering is isotropic, indicative of a long-lived collision complex. The energy transfer distribution agrees very well with that predicted by phase space theory (PST),[9] which assumes a $ClCH_3$---I^- postreaction complex with statistical unimolecular dynamics. Increasing E_{rel} to 0.76 eV retains an isotropic component in the scattering, but backward scattering now dominates. At 1.07 eV, there is only backward scattering, with no isotropic component. Interestingly, with E_{rel} further increased to 1.9 eV, there is now a small component in the scattering with low product translational energies, as expected for complex formation.

Direct dynamics simulations were performed[8,27] to interpret the I^- scattering observed in the experiments. Initial conditions were chosen for the simulation trajectories to match those for the experiments. Excellent agreement with experiment was found for the simulations at 0.76, 1.07, and 1.9 eV. As shown in Table 2, the fraction of the available energy transferred to CH_3I rovibration, f_{int}, is statistically the same for the simulations and experiments.

The simulations provide an atomistic understanding of the scattering. For the 1.9 eV collisions, 82% of the reaction is direct, with 73% rebound and 9% stripping. The remaining 18% of the reaction is indirect and occurs by a pathway not previously identified, called the roundabout mechanism (see Figure 3). For this mechanism, Cl^- first strikes the side of CH_3, causing it to rotate about the massive I atom. Then, after one CH_3 rotation, Cl^- attacks the C atom backside and directly displaces I^-. Variants of this mechanism, of much less importance, include trapping of I^- in the postreaction complex and/or multiple rotations of the CH_3 group about the I atom. At 1.07 eV, all of the reaction occurs by direct rebound. At the 0.76 eV collision energy, 87% of the reaction occurs by direct rebound. The remainder is indirect.

In contrast to the isotropic and indirect experimental scattering dynamics at 0.39 eV, the simulations indicate the reaction is dominated by direct processes as found for the higher E_{rel}. The fraction of the available energy partitioned to f_{int} is 0.51 ± 0.04 in the simulations, but ∼0.84 in the experiments. Decreasing the simulation E_{rel} to 0.20 eV results in product energy partitioning and scattering which agree with the 0.39 eV experiment; that is, the simulation f_{int} becomes 0.86 ± 0.03. The simulations' lack of agreement with the 0.39 eV experiment may result from a distribution of collision energies in the experiment and/or a shortcoming in the direct dynamics simulations. The sharp transition from a 99% direct to 83% indirect reaction as E_{rel} is lowered from 0.39 to 0.20 eV in the simulations is striking. It is of interest that earlier studies for the $Cl^- + CH_3Cl$[24,25] and $Cl^- + CH_3Br$[23,26] S_N2 reactions indicate that their reaction mechanisms change from predominantly indirect to direct at E_{rel} of approximately 0.48 and 0.30 eV, respectively.

The change in the atomistic mechanisms with increase in E_{rel} and the indirect roundabout mechanism at high E_{rel} are intriguing aspects of the $Cl^- + CH_3I$ S_N2 dynamics. The roundabout mechanism partitions a large fraction of the product energy to CH_3Cl rovibration, in approximate agreement with PST. However, the energy transfer dynamics are not statistical and instead involve near adiabatic $CH_3I \rightarrow CH_3Cl$ rotational and C−I → C−Cl stretch vibrational energy transfer. Angular momentum is conserved as the CH_3-group rotates around the I atom and this rotational energy is transferred to CH_3Cl rotation.

B. $F^- + CH_3I$ Reaction Dynamics

The $F^- + CH_3I$ reaction dynamics are decidedly different from those for $Cl^- + CH_3I$.[28,29] A major difference is that there is not a sharp transition from an indirect to direct reaction as E_{rel} is increased. This is illustrated in Figure 4 where the measured relative velocity images of I^- are presented for $F^- + CH_3I \rightarrow FCH_3 + I^-$ reactive scattering.[29] Also given are distributions of the available product energy released to FCH_3 rovibrational internal energy. The scattering is approximately isotropic at 0.32 and 0.69 eV, and then backward scattering becomes pronounced at the higher E_{rel}. However, at each E_{rel}, scattering events are important for which all the available product energy is transferred to FCH_3 rovibrational energy, f_{int}. The average value of f_{int} slightly decreases from 0.70 ± 0.09 to 0.62 ± 0.07 as E_{rel} is increased from 0.32 to 2.34 eV. Such large fractions are indicative

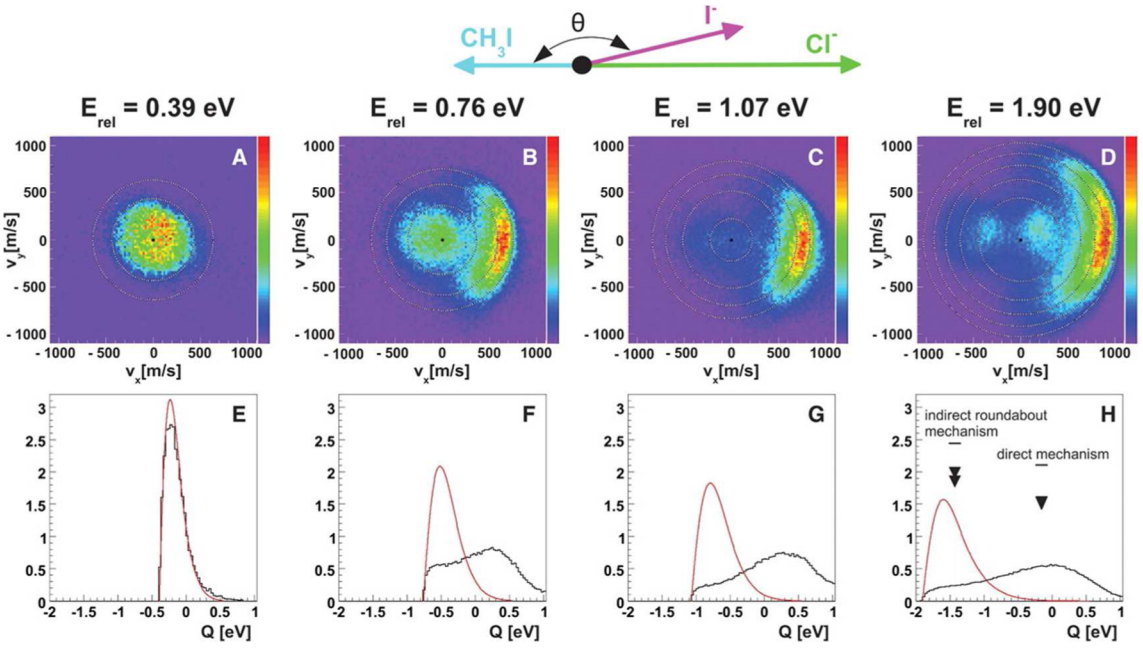

Figure 2. (A–D) Center-of-mass images of the I^- product velocity from the reaction of Cl^- with CH_3I at four different E_{rel}. The image intensity is proportional to $[(d^3\sigma)/(dvx\, dvy\, dvz)]$: Isotropic scattering results in a homogeneous ion distribution on the detector. (E–H) The energy transfer distributions extracted from the images in (A–D) in comparison with a PST calculation (red curve). The arrows in (H) indicate the average Q values obtained from the direct dynamics simulations. Adapted with permission from ref 8. Copyright 2008 by the American Association for the Advancement of Science.

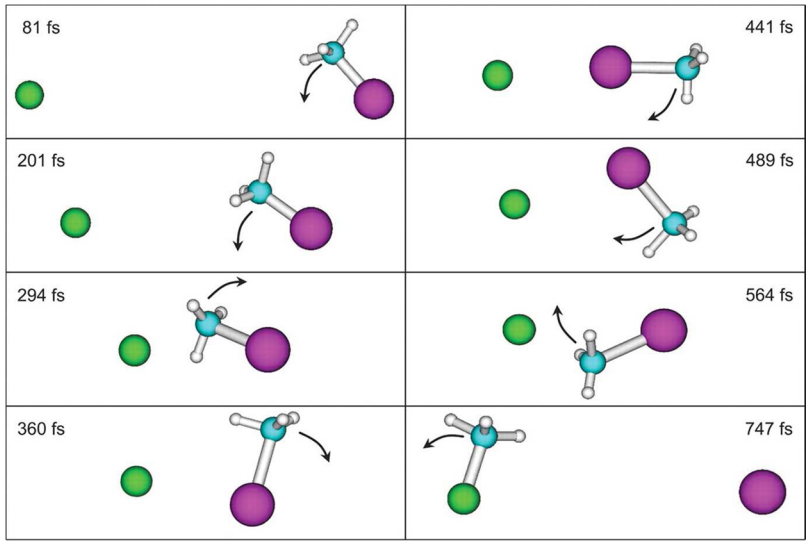

Figure 3. View of a typical trajectory for the indirect roundabout reaction mechanism at 1.9 eV. Adapted with permission from ref 8. Copyright 2008 by the American Association for the Advancement of Science.

of an appreciable indirect, isotropic component in the reaction dynamics.

The minimum in each scattering angle distribution in Figure 4 may be used to identify a maximum isotropic component, which is assumed to have the same probability at each scattering angle, for example, 0.33 for E_{rel} of 0.32 eV. The resulting estimated fraction of the isotropic scattering is 0.66, 0.72, 0.44, 0.39, and 0.30 for E_{rel} of 0.32, 0.69, 1.53, 1.81, and 2.34 eV, respectively. The isotropic component decreases with increasing E_{rel}, but remains appreciable at the highest E_{rel}, consistent with the large f_{int}.

Electronic structure calculations[36] and direct dynamics simulations[28,29] were performed to complement the experiments. A significant finding, shown in Figure 5, is that the PES for the $F^- + CH_3I$ S_N2 reaction is substantially different from that for $Cl^- + CH_3I$. There is a hydrogen-bonded prereaction complex F^----HCH_2I and transition state $[F\text{--}HCH_2\text{--}I]^-$. At the DFT/B97-1 level of theory, these are the only prereaction stationary points, the same result obtained with other DFT functionals. In contrast, MP2 theory gives these stationary points as well as the traditional C_{3v} prereaction complex and central barrier. Initial CCSD(T) energy scans[36] indicated the B97-1 PES was correct and it was used for the direct dynamics simulations, but recent more complete CCSD(T) calculations[37] find the same stationary points as for the MP2 PES. However, both the B97-1 and MP2 PESs are rather flat in the prereaction region, with low barriers

dx.doi.org/10.1021/ar5001764 | Acc. Chem. Res. 2014, 47, 2960–2969

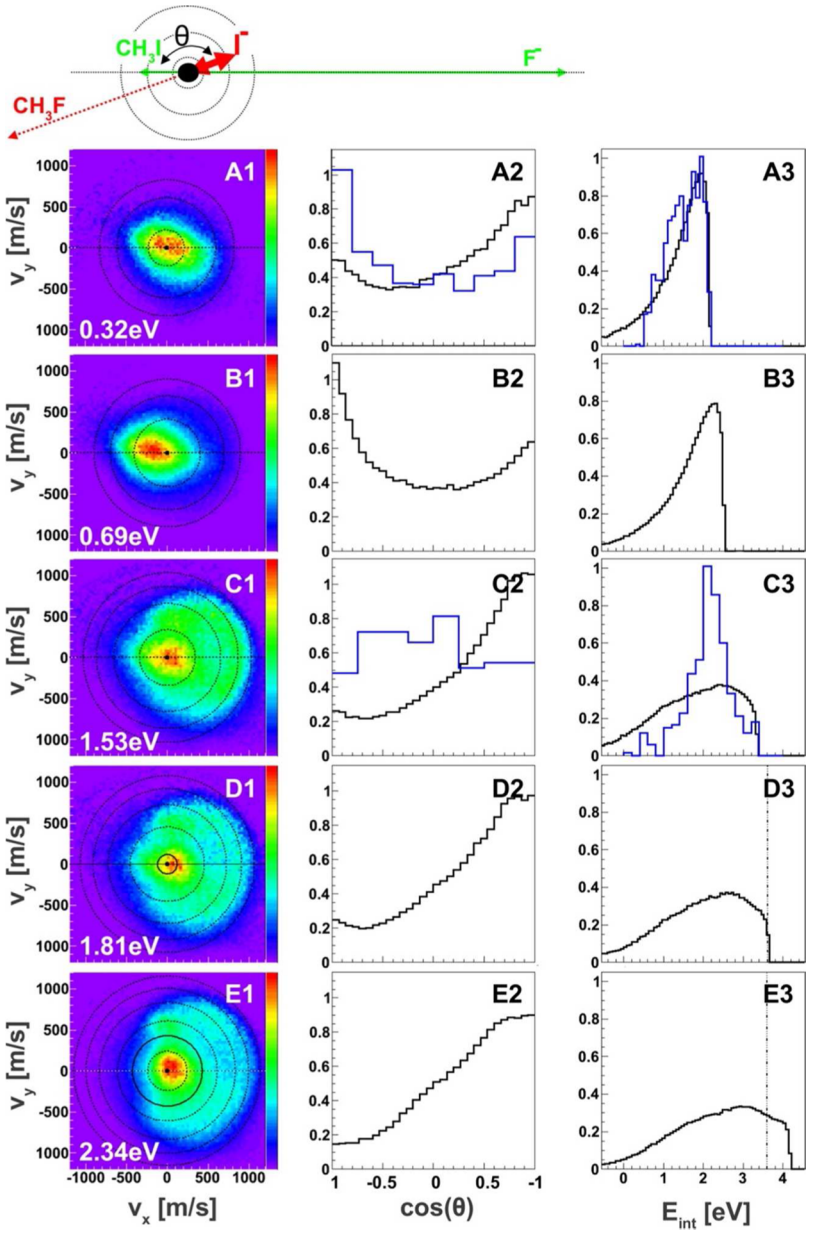

Figure 4. (A1−E1) Measured velocity images of the I^- product from reactive scattering of F^- and CH_3I at different collision energies (see the schematic Newton diagram in the center-of-mass frame at the top). (A2−E2) and (A3−E3) Histograms of the scattering angle and the internal excitation (black) for the same relative collision energies as in (A1−E1). The E_{int}-histograms show a sharp upper bound, caused by products with vanishing velocity, and a more diffuse lower bound, due to the finite energy resolution. Simulation results for 0.32 and 1.53 eV are shown in blue. Adapted with permission from ref 29. Copyright 2013 American Chemical Society.

from the prereaction complex to the FCH_3---I^- postreaction complex.

B97-1/ECP/d direct dynamics were used to simulate the atomistic dynamics for the F^- + CH_3I S_N2 reaction.[28,29] The calculations were performed at the low and high E_{rel} of 0.32 and 1.53 eV to compare with the experiments. Fractions of the different atomistic mechanisms are summarized in Table 2. Though the barrier is quite low for the F^----HCH_2I prereaction complex to pass the TS and form products, ~60% of the reaction is indirect. The remaining reaction occurs by direct rebound and stripping. The large fraction of the indirect reaction is in qualitative agreement with the isotropic scattering observed in the experiments. At 0.32 and 1.53 eV, respectively, 98% and 95% of the indirect reaction involves formation of the prereaction complex.

As shown in Table 2, there is quantitative agreement between the experimental and simulation average fractions of the energy partitioned to CH_3F internal energy for both the 0.32 and 1.53 eV collisions. As shown in Figure 4, such agreement is also found between the product energy distributions at 0.32 eV. For the 1.53 eV collisions, experiment finds a significantly larger probability for low internal energies than the simulations.

For the 0.32 eV collisions, the velocity scattering angle distribution from the simulations (Figure 4) is in overall agreement with experiment, but the simulation scattering is most probable for forward scattering with $\theta = 0°$, while the experimental scattering is most probable for backward scattering with $\theta = 180°$. The rather isotropic scattering in the simulations is a composite of stripping (forward), rebound (backward), and indirect (isotropic). The difference between experiment and simulation is

dx.doi.org/10.1021/ar5001764 | Acc. Chem. Res. 2014, 47, 2960−2969

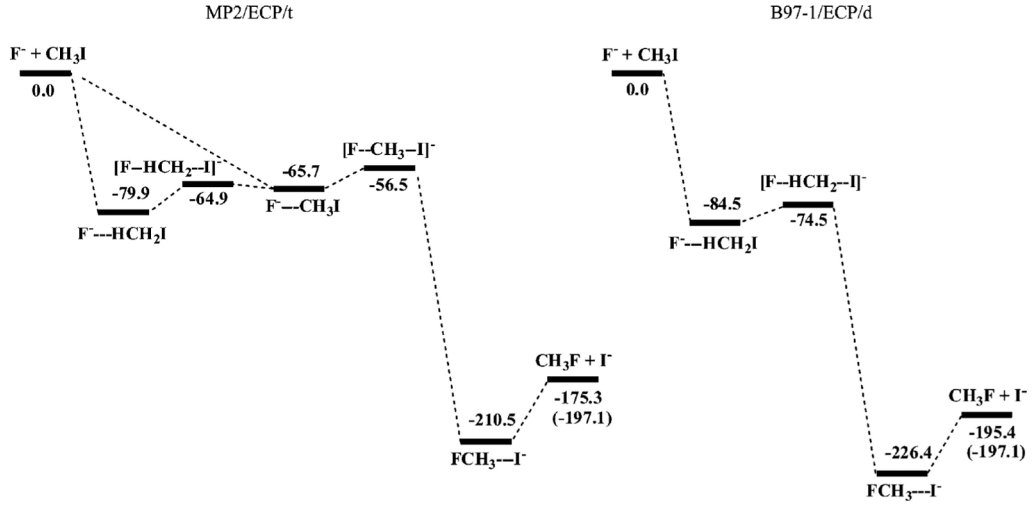

Figure 5. Potential energy curves and stationary points for the MP2/ECP/t and B97−1/ECP/d PESs. The experimental reaction exothermicity is in parentheses. The energy in kJ/mol is relative to the F^- + CH_3I reactants and does not include ZPEs. Adapted with permission from ref 36. Copyright 2010 American Chemical Society..

more pronounced at 1.53 eV, where the simulation scattering is nearly isotropic, while experimentally backward scattering is most probable. This difference is also observed in the product energy distributions, where low product internal energies produced by backward scattering are absent in the simulations.

As discussed above, the B97-1/ECP/d PES used for the simulations has only the hydrogen-bonded entrance channel,[36] while the higher level CCSD(T) PES has both this and the traditional C_{3v} entrance channels.[37] It might be expected that this difference would manifest itself at low collision energies. However, at 0.32 eV, the dynamics given by the B97-1 PES are in overall good agreement with experiment. It is at the higher collision energy of 1.53 eV where the difference in the B97-1/ECP/d and experimental dynamics become more significant. Apparently, there are high energy regions of the B97-1/ECP/d PES which are inaccurate.

C. OH^- + CH_3I

The experimental scattering images for the OH^- + CH_3I S_N2 reaction[33] in Figure 6 are strikingly different from those for F^- + CH_3I in Figure 4. The dominant feature in these images is scattering in the forward hemisphere, characteristic of stripping. Backward scattering for the rebound mechanism is a minor channel, as is scattering to products with low translational energy. The latter is a component of the indirect mechanism. The images were analyzed to determine the fractional ratio forward/backward/(low energy),[33] which is 0.66:0.28:0.06, 0.61:0.33:0.06, 0.60:0.35:0.05, and 0.63:0.30:0.07 for collision energies of 0.5, 1.0, 1.5, and 2.0 eV, respectively. In contrast to these fractions, the F^- + CH_3I S_N2 scattering dynamics is primarily backward with an appreciable low energy component.

The B97-1/ECP/d method was used to characterize the OH^- + CH_3I PES (Figure 7) and to perform the direct dynamics.[30,31] As found for the F^- + CH_3I reaction, this method gives only the hydrogen-bonded entrance channel reaction pathway. However, in contrast to F^- + CH_3I, this is also the finding with MP2/ECP and the double- and triple-ζ basis sets. Apparently, OH^- + CH_3I does not have the C_{3v} entrance channel reaction pathway. The entrance channel energetics are very similar for the F^- + CH_3I and OH^- + CH_3I reactions. For both (X = F, OH), the energy of the X^----HCH_2I prereaction complex is −20 kcal/mol with respect to the reactants and that of the $[X\text{--}HCH_2\text{--}I]^-$ TS is −18 kcal/mol.

As shown in Table 2, for E_{rel} of 1.0 and 2.0 eV, the atomistic mechanism probabilities determined from the simulations are in near quantitative agreement with those above for the experiments. At 0.5 eV, the simulation probability for stripping is smaller and that for indirect is larger than deduced from the experiments. What is remarkable is that, though OH^- + CH_3I and F^- + CH_3I have similar S_N2 potential energy curves, their reaction dynamics are much different.

D. $OH^-(H_2O)_{n=1,2}$ + CH_3I

As first step to bridge the gap between gas phase and solution, microsolvated systems were studied.[32,33] With the stepwise addition of solvent molecules to the bare reactant, anion microsolvation offers a bottom up approach to learn more about the transition of chemical reactions from the gas to liquid phase. The production of selectively solvated species like $OH^-(H_2O)_n$ can be easily achieved, and the chemistry of these systems may be studied as a function of solvation number. For a more detailed study of solvation, it will be important to consider solvation of both reactants, that is, CH_3I as well as OH^-. The current study is a first step and considers the reactant which interacts more strongly with H_2O. The studies focus on water, since it is the most important liquid phase for chemical reactions on earth.

The reaction $OH^-(H_2O)_{n=1,2}$ + CH_3I was studied at E_{rel} of 0.5, 1.0, 1.5, and 2.0 eV, and the experimental scattering images are shown in Figure 6.[33] The dynamics observed $OH^-(H_2O)$ differ quite dramatically from the unsolvated system. For the unsolvated reaction the indirect mechanism is of minor importance, with preferential scattering into the forward hemisphere. In contrast, for monosolvated OH^-, the indirect mechanism becomes important and the measured velocity angular distribution is almost isotropic at low energies. However, the dynamics switches to backward scattering for the rebound mechanism at collision energies above 1 eV. At all energies a large fraction of the available energy is partitioned to internal energy of the products.

Electronic structure calculations[33] were used to identify the structure for the $OH^-(H_2O)$ + CH_3I reaction's entrance channel complex. In contrast to the hydrogen-bonded HO^----HCH_2I

dx.doi.org/10.1021/ar5001764 | Acc. Chem. Res. 2014, 47, 2960−2969

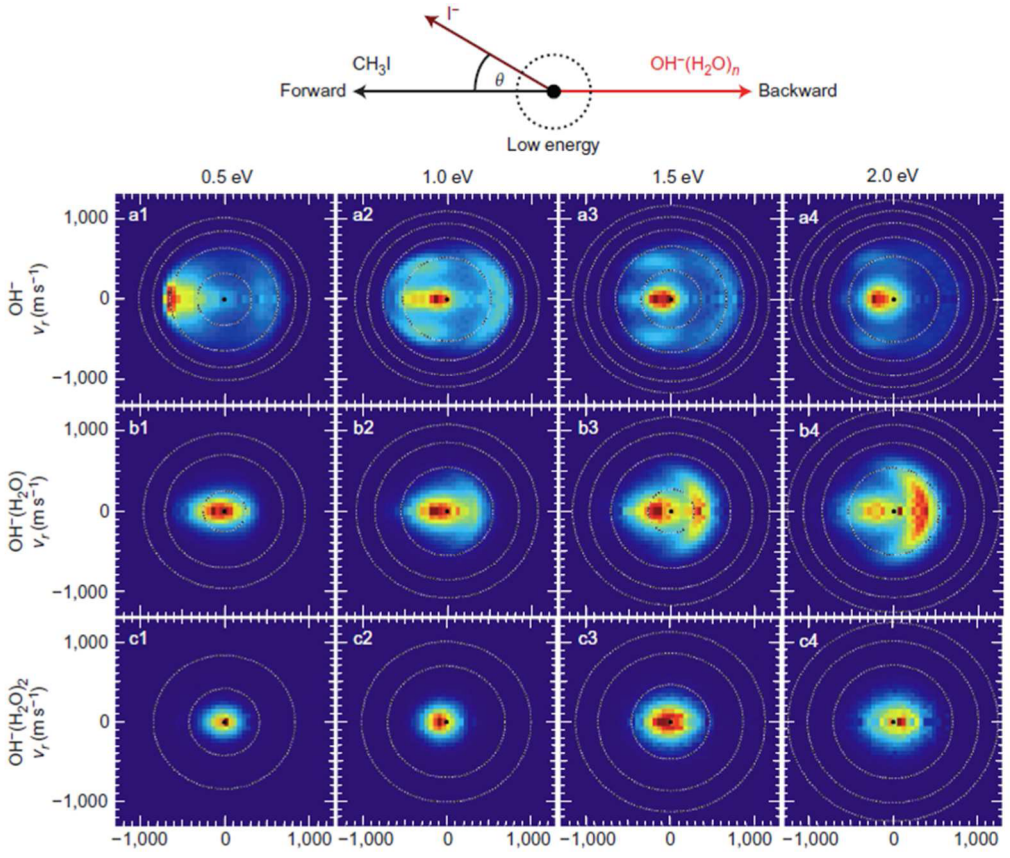

Figure 6. Twelve panels show the velocity distributions of the I^- products in the scattering plane for the reactions $OH^-(H_2O)_n + CH_3I$, $n = 0, 1, 2$, at E_{rel} of 0.5−2.0 eV. The measured distributions represent the differential scattering cross sections. Different dynamical features may be distinguished, which include mechanisms with forward scattering, backward scattering, and the formation of low-energy products. Adapted with permission from ref 33. Copyright 2012 by the Nature Publishing Group.

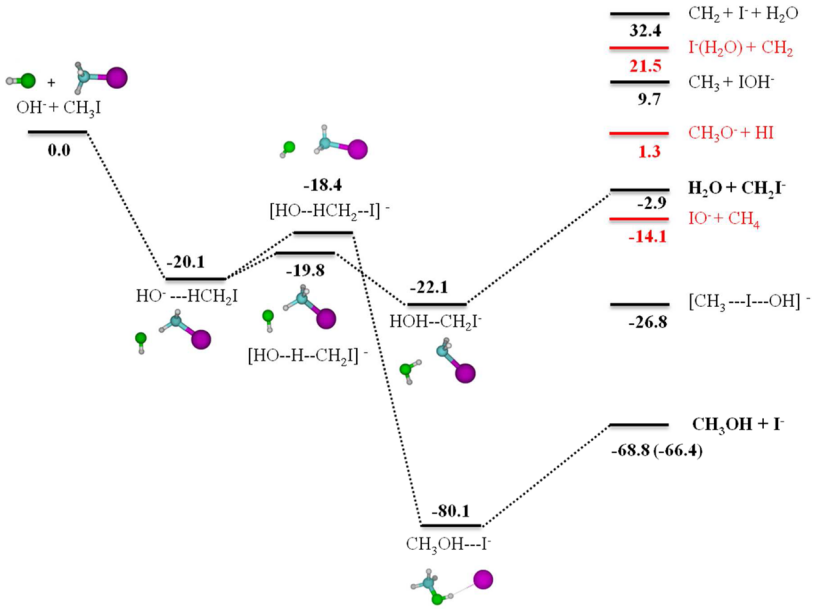

Figure 7. DFT/B97-1/ECP/d energy profile for the $OH^- + CH_3I \rightarrow CH_3OH + I^-$ and $OH^- + CH_3I \rightarrow CH_2I^- + H_2O$ reactions, and other possible reaction channels. The energies are in kcal/mol and are relative to the $OH^- + CH_3I$ reactants. Zero point energies are not included. Experimental 0 K heats of reaction are in parentheses. The products in red were not observed in either the simulations or experiments.

complex for the unsolvated reaction,[30] for the solvated reaction, the complex is similar to the traditional C_{3v} structure with OH^- almost collinear with the C−I axis. The geometry of the complex favors a direct backside encounter, promoting the rebound mechanism. That the S_N2 mechanism is not suppressed, and the rebound mechanism becomes dominant above 1.0 eV, is

dx.doi.org/10.1021/ar5001764 | Acc. Chem. Res. 2014, 47, 2960−2969

indicative of a steering role of this entrance channel complex for backside attack.

Figure 6 shows that adding a second water molecule to the reactant ion suppresses all angle-dependent features in the scattering. The $OH^-(H_2O)_2$ + CH_3I reaction leads to isotropically distributed products with small absolute velocities for all collision energies and shows no evidence for direct S_N2 reaction. Electronic structure calculations[33] find an entrance channel complex that fixes the central OH^- anion further away from the CH_3I than for $OH^-(H_2O)$ or bare OH^-. The solvent water molecules have to be pushed aside or rearranged in a collision complex before the OH^- can attack CH_3I. It is possible that in such reactive events a major part of the collision energy is transferred into internal energy, which may explain the measured high internal excitation in the product molecules.

Solvating the reactant species opens up new S_N2 pathways leading to solvated products.[32,33] For the $OH^-(H_2O)$ + CH_3I reaction, the $I^-(H_2O)$ product is observed. Although the pathway for this product is 0.4 eV more exothermic than that for the I^- pathway, the former is strongly suppressed. Analyzing the velocity distributions for this solvated S_N2 channel reveals purely complex mediated reaction dynamics at all energies, in strong contrast to the direct rebound mechanism that dominates the formation of unsolvated I^-. Strong interactions in the reaction's exit channel may explain this finding.[34]

III. COMPARISONS OF THE REACTION DYNAMICS

A remarkable feature of the S_N2 reactions studied here are their range of atomistic mechanisms, which differ for each of the reactions (Table 2). At low collision energy, E_{rel}, the Cl^- + CH_3I reaction occurs by the traditional model in eq 1, in which a prereaction ion-dipole complex, Cl^----CH_3I, is formed.[8,27] However, at E_{rel} of ∼0.2−0.4 eV the reaction becomes direct, without complex formation, occurring by the rebound mechanism with backward scattering. At a high E_{rel} of 1.9 eV the roundabout mechanism contributes to the reaction.

For the F^- + CH_3I reaction there is not a transition from indirect to direct reaction as E_{rel} is increased.[29] The indirect mechanism, with prereaction complex formation, is important at all the E_{rel} investigated, contributing up ∼60% of the reaction. The remaining direct reaction occurs by the rebound and stripping mechanisms.

Though the S_N2 potential energy curve for the OH^- + CH_3I reaction is similar to that for F^- + CH_3I, the two reactions have different dynamics.[30,33] They are akin, in that for both there is not a transition from an indirect to direct reaction. However, for F^- + CH_3I indirect reaction dominates at all E_{rel}, but it is less important for OH^- + CH_3I and becomes negligible as E_{rel} is increased. Stripping is a minor channel for F^- + CH_3I, but accounts for more than 60% of the OH^- + CH_3I reaction at high E_{rel}. Origins of the different S_N2 dynamics for the OH^- + CH_3I and F^- + CH_3I reactions are uncertain, but they are clearly related to differences in the PESs for the two reactions. Examples of these differences are the coupling between the S_N2 and proton-transfer pathways and importance of the $[CH_3$--I--$OH]^-$ intermediate for the OH^- + CH_3I reactions,[30,31] dynamics that are not important for the F^- + CH_3I reaction.

Adding either one or two H_2O molecules to OH^- alters the reaction dynamics from that for unsolvated OH^-.[32,33] Adding one H_2O molecule enhances indirect reaction at low E_{rel}, and changes the reaction mechanism from primarily stripping to rebound at high E_{rel}. With two H_2O molecules, the dynamics is indirect and isotropic at all collision energies.

PST assumes a long-lived $XCH_3{-}Y^-$ postreaction complex, with statistical dynamics giving rise to statistical product energies.[9] Though PST product energy distributions are observed for some reaction conditions, the simulation dynamics are inconsistent with the PST model. For the Cl^- + CH_3I simulations at 0.20 eV,[27] product energies agree with PST, but only 50% of the reactive trajectories form the postreaction complex. For F^- + CH_3I at 0.32 eV, product energies are very similar to PST, but a postreaction complex is formed in only 7% of the reactive events.[28,29] Apparently, statistical-like product energy partitioning does not require postreaction complex formation and instead, in moving from the central TS to products, potential energy may be released in a statistical manner. The relationship between statistical product energy partitioning and nonstatistical unimolecular dissociation dynamics has been considered previously.[38]

IV. FUTURE DIRECTIONS

In future work, it will be important to obtain understanding of the origins of the above changes in the S_N2 dynamics for the X^- + CH_3Y reactions. The roundabout mechanism has features similar to the roaming mechanism,[39−41] and it would be of interest to carefully compare the dynamics for the roaming reaction with the roundabout's nonstatistical dynamics. Also of interest is attaining a clearer picture of how microsolvation alters the reaction dynamics and its connection to the solution-phase kinetics. The α-effect in S_N2 reaction dynamics could also be studied.[42] The H_2O---CH_2I^- complex participates in the OH^- + CH_3I S_N2 reaction (Figure 7), and the importance of this proton-transfer for the S_N2 pathway could be investigated by studying the reaction of OD^- and the branching between the CH_3OD and CH_2DOH S_N2 products. For the simulations, it will be important to consider additional electronic structure methods for the direct dynamics and interpolation procedures for enhancing the simulations.[43] Analytic PESs may also be used.[44]

There are other pathways for X^- + CH_3Y reactions besides S_N2 nucleophilic substitution. For F^- + CH_3I, the proton-transfer products HF + CH_2I^- become energetically accessible at E_{rel} of 0.6 eV.[29] As shown in Figure 7, for OH^- + CH_3I, there are eight possible product channels, of which only five are observed in the experiments and simulations.[30−33] For this reaction, the S_N2 and proton-transfer pathways have nearly equal importance.[30,31] Unraveling the dynamics for the different OH^- + CH_3I pathways, and their couplings, is certainly of interest. For a larger alkyl group, there is also the E2 pathway forming H_2O + C_2H_4 + I^- for HO^- + C_2H_5I.[4] Simulations and experiments of this reaction would be of considerable interest, as well as for larger systems such as secondary and tertiary alkyl halides. Though it is difficult to predict the atomistic dynamics for these reactions and their relations to the dynamics described here, the current work will be very beneficial for interpreting the results of these future studies.

■ AUTHOR INFORMATION

Corresponding Author

*E-mail: bill.hase@ttu.edu.

Notes

The authors declare no competing financial interest.

Biographies

Jing Xie received her B.S. degree in Chemistry from Beijing Normal University, Beijing, China, in 2010. She is a Ph.D. candidate in chemistry at Texas Tech University under the direction of William L. Hase. Her

research is focused on classical and semiclassical direct dynamics simulations.

Rico Otto obtained a Diploma in 2006 and a Ph.D. in Physics in 2011 from the Albert-Ludwigs-University in Freiburg, Germany, the latter under the direction of Roland Wester. Since 2011, he has carried out postdoctoral research at the University of California, San Diego with Robert Continetti.

Jochen Mikosch received a M.S. in Theoretical Physics in 2002 from the University of Cambridge (U.K.) and a Ph.D. from the University of Freiburg in 2007. He then worked as a Research Associate at the National Research Council in Ottawa, Canada on time-resolved photoelectron spectroscopy and strong-field ionization of molecules. Jochen recently moved to the Max-Born-Institute in Berlin, where he joined an Attosecond Physics division.

Jiaxu Zhang received his Ph.D. degree from Jilin University in China in 2006, and was a postdoctoral research associate at Texas Tech University from 2006 to 2011 and Virginia Tech from 2011 to 2012. In October 2012, he became an Associate Professor at the Institute of Chemistry, Chinese Academy of Sciences. In 2014, he moved to the Harbin Institute of Technology as a Professor. His research interests focus on electronic structure theory and chemical dynamics calculations of physically and chemically important reactions and phenomena.

Roland Wester studied Physics at the Universities of Konstanz and Heidelberg, and received his Ph.D. from the University of Heidelberg in 1999 for Coulomb explosion imaging experiments of molecular ions. He then worked for 2 years at the University of California in Berkeley on femtosecond spectroscopy. From 2003 to 2010, he was at the University of Freiburg, before becoming a Professor at the University of Innsbruck. His main field of research is the study of interactions and reaction dynamics of cold molecules and molecular ions.

William L. Hase received a B.S. in Chemistry from University of Missouri, Columbia in 1967 and a Ph.D. in Physical Chemistry from New Mexico State University in 1970. He joined the faculty at Wayne State University in 1973 after a postdoctoral at University of California, Irvine. In 2004, he assumed the Welch Chair in Chemistry at Texas Tech University.

■ ACKNOWLEDGMENTS

The research at Texas Tech University is supported by the Robert A. Welch Foundation. J.M., R.O., and R.W. thank their co-workers in the crossed-beam imaging experiments. The experimental research has been and is supported by the Deutsche Forschungsgemeinschaft (DFG) and the Austrian Science Fund (FWF). J.Z. thanks the Fundamental Research Funds for the Central Universities, China (AUGA5710012114) for support of his research.

■ REFERENCES

(1) Ingold, C. K. *Structure and Mechanism in Organic Chemistry*; Cornell University Press: Ithaca, NY, 1953.
(2) Olmstead, W. N.; Brauman, J. I. Gas-phase Nucleophilic Displacement Reactions. *J. Am. Chem. Soc.* **1977**, *99*, 4219−4228.
(3) Ritchie, C. D.; Chappel, G. A. Ab Initio LCGO-MO-SCF Calculation of the Potential Energy Surface for an S_N2 Reaction. *J. Am. Chem. Soc.* **1970**, *92*, 1819−1821.
(4) DePuy, C. H.; Gronert, S.; Mullin, A.; Bierbaum, V. M. Gas-Phase S_N2 and E2 Reactions of Alkyl Halides. *J. Am. Chem. Soc.* **1990**, *112*, 8650−8655.
(5) Chabinyc, M. L.; Craig, S. L.; Regan, C. K.; Brauman, J. I. Gas-Phase Ionic Reactions: Dynamics and Mechanism of Nucleophilic Displacements. *Science* **1998**, *279*, 1882−1886.
(6) Laerdahl, J. K.; Uggerud, E. Gas Phase Nucleophilic Substitution. *Int. J. Mass Spectrom.* **2002**, *214*, 277−314.
(7) Manikandan, P.; Zhang, J.; Hase, W. L. Chemical Dynamics Simulations of $X^- + CH_3Y \rightarrow XCH_3 + Y^-$ Gas-Phase S_N2 Nucleophilic Substitution Reactions. Nonstatistical Dynamics and Nontraditional Reaction Mechanisms. *J. Phys. Chem. A* **2012**, *116*, 3061−3080.
(8) Mikosch, J.; Trippel, S.; Eichhorn, C.; Otto, R.; Lourderaj, U.; Zhang, J. X.; Hase, W. L.; Weidemüller, M.; Wester, R. Imaging Nucleophilic Substitution Dynamics. *Science* **2008**, *319*, 183−186.
(9) Baer, T.; Hase, W. L. *Unimolecular Reaction Dynamics. Theory and Experiments*; Oxford: New York, 1996.
(10) Vande Linde, S. R.; Hase, W. L. A Direct Mechanism for S_N2 Nucleophilic Substitution Enhanced by Mode-selective Vibrational Excitation. *J. Am. Chem. Soc.* **1989**, *111*, 2349−2351.
(11) Vande Linde, S. R.; Hase, W. L. Non-RRKM Kinetics in Gas-phase S_N2 Nucleophilic Substitution. *J. Phys. Chem.* **1990**, *94*, 6148−6150.
(12) Hase, W. L. Simulations of Gas-Phase Chemical Reactions: Applications to S_N2 Nucleophilic Substitution. *Science* **1994**, *266*, 998−1002.
(13) Wester, R.; Bragg, A. E.; Davis, A. V.; Neumark, D. M. Time-resolved study of the symmetric S_N2-reaction $I^- + CH_3I$. *J. Chem. Phys.* **2003**, *119*, 10032−10039.
(14) Li, C.; Ross, P.; Szulejko, J. E.; McMahon, T. B. High-Pressure Mass Spectrometric Investigations of the Potential Energy Surfaces of Gas-Phase S_N2 Reactions. *J. Am. Chem. Soc.* **1996**, *118*, 9360−9367.
(15) Mikosch, J.; Otto, R.; Trippel, S.; Eichhorn, C.; Weidemüller, M.; Wester, R. Inverse Temperature Dependent Lifetimes of Transient S_N2 Ion-Dipole Complexes. *J. Phys. Chem. A* **2008**, *112*, 10448−10452.
(16) Tonner, D. S.; McMahon, T. B. Non-Statistical Effects in the Gas Phase S_N2 Reaction. *J. Am. Chem. Soc.* **2000**, *122*, 8783−8784.
(17) Viggiano, A. A.; Paschkewitz, J.; Morris, R. A.; Paulson, J. F.; Gonzalez-Lafont, A.; Truhlar, D. G. Temperature Dependence of the Kinetic Isotope Effect for a Gas-phase S_N2 Reaction: $Cl^- + CH_3Br$. *J. Am. Chem. Soc.* **1991**, *113*, 9404−9405.
(18) Le Garrec, J.-L.; Rowe, B. R.; Queffelec, J. L.; Mitchell, J. B. A.; Clary, D. C. Temperature Dependence of the Rate Constant for the $Cl^- + CH_3Br$ Reaction Down to 23 K. *J. Chem. Phys.* **1997**, *107*, 1021−1024.
(19) Wang, H.; Hase, W. L. Statistical Rate Theory Calculations of the $Cl^- + CH_3Br \rightarrow ClCH_3 + Br^-$ Rate Constant Versus Temperature, Translational Energy, and H(D) Isotopic Substitution. *J. Am. Chem. Soc.* **1995**, *117*, 9347−9356.
(20) Viggiano, A. A.; Morris, R. A.; Paschkewitz, J. S.; Paulson, J. F. Kinetics of the Gas-phase Reactions of Chloride Anion, Cl^- with CH_3Br and CD_3Br: Experimental Evidence for Nonstatistical Behavior? *J. Am. Chem. Soc.* **1992**, *114*, 10477−10482.
(21) Craig, S. L.; Brauman, J. I. Phase-Shifting Acceleration of Ions in an Ion Cyclotron Resonance Spectrometer: Kinetic Energy Distribution and Reaction Dynamics. *J. Phys. Chem. A* **1997**, *101*, 4745−4752.
(22) Graul, S. T.; Bowers, M. T. Vibrational Excitation in Products of Nucleophilic Substitution: The Dissociation of Metastable $X^-(CH_3Y)$ in the Gas Phase. *J. Am. Chem. Soc.* **1994**, *116*, 3875−3883.
(23) Angel, L. A.; Ervin, K. M. Gas-Phase S_N2 and Bromine Abstraction Reactions of Chloride Ion with Bromomethane: Reaction Cross Sections and Energy Disposal into Products. *J. Am. Chem. Soc.* **2003**, *125*, 1014−1027.
(24) DeTuri, V. F.; Hintz, P. A.; Ervin, K. M. Translational Activation of the S_N2 Nucleophilic Displacement Reactions $Cl^- + CH_3Cl$ $(CD_3Cl) \rightarrow ClCH_3$ $(ClCD_3) + Cl^-$: A Guided Ion Beam Study. *J. Phys. Chem. A* **1997**, *101*, 5969−5986.
(25) Mann, D. J.; Hase, W. L. Trajectory Studies of S_N2 Nucleophilic Substitution. 6. Translational Activation of the $Cl^- + CH_3Cl$ Reaction. *J. Phys. Chem. A* **1998**, *102*, 6208−6214.
(26) Wang, Y.; Hase, W. L.; Wang, H. Trajectory Studies of S_N2 Nucleophilic Substitution. IX. Microscopic Reaction Pathways and Kinetics for $Cl^- + CH_3Br$. *J. Chem. Phys.* **2003**, *118*, 2688−2695.
(27) Zhang, J.; Lourderaj, U.; Sun, R.; Mikosch, J.; Wester, R.; Hase, W. L. Simulation Studies of the $Cl^- + CH_3I$ S_N2 Nucleophilic Substitution

Reaction: Comparison with Ion Imaging Experiments. *J. Chem. Phys.* **2013**, *138*, 114309.
(28) Zhang, J.; Mikosch, J.; Trippel, S.; Otto, R.; Weidemüller, M.; Wester, R.; Hase, W. L. $F^- + CH_3I \rightarrow FCH_3 + I^-$ Reaction Dynamics. Nontraditional Atomistic Mechanisms and Formation of a Hydrogen-Bonded Complex. *J. Phys. Chem. Lett.* **2010**, *1*, 2747−2752.
(29) Mikosch, J.; Zhang, J.; Trippel, S.; Eichhorn, C.; Otto, R.; Sun, R.; de Jong, W. A.; Weidemüller, M.; Hase, W. L.; Wester, R. Indirect Dynamics in a Highly Exoergic Substitution Reaction. *J. Am. Chem. Soc.* **2013**, *135*, 4250−4259.
(30) Xie, J.; Sun, R.; Siebert, M. R.; Otto, R.; Wester, R.; Hase, W. L. Direct Dynamics Simulations of the Product Channels and Atomistic Mechanisms for the $OH^- + CH_3I$ Reaction. Comparison with Experiment. *J. Phys. Chem. A* **2013**, *117*, 7162−7178.
(31) Xie, J.; Kohale, S. C.; Hase, W. L.; Ard, S. G.; Melko, J. J.; Shuman, N. S.; Viggiano, A. A. Temperature Dependence of the $OH^- + CH_3I$ Reaction Kinetics. Experimental and Simulation Studies and Atomic-Level Dynamics. *J. Phys. Chem. A* **2013**, *117*, 14019−14027.
(32) Otto, R.; Xie, J.; Brox, J.; Trippel, S.; Stei, M.; Best, T.; Siebert, M. R.; Hase, W. L.; Wester, R. Reaction Dynamics of Temperature-Variable Anion Water Clusters Studied with Crossed Beams and by Direct Dynamics. *Faraday Discuss.* **2012**, *157*, 41−57.
(33) Otto, R.; Brox, J.; Stei, M.; Trippel, S.; Best, T.; Wester, R. Single Solvent Molecules can Affect the Dynamics of Substitution Reactions. *Nat. Chem.* **2012**, *4*, 534−538.
(34) Otto, R.; Brox, J.; Trippel, S.; Best, T.; Wester, R. Exit Channel Dynamics in a Micro-Hydrated S_N2 Reaction of the Hydroxyl Anion. *J. Phys. Chem. A* **2013**, *117*, 8139−8144.
(35) Henglein, V. A.; Lacmann, K.; Jacobs, G. Zum Sto*β*mechanismus Bimolekularer Reaktiònen. *Ber. Bunsen-Ges.* **1965**, *69*, 279−286.
(36) Zhang, J.; Hase, W. L. Electronic Structure Theory Study of the $F^- + CH_3I \rightarrow FCH_3 + I^-$ Potential Energy Surface. *J. Phys. Chem. A* **2010**, *114*, 9635−9643.
(37) Sun, R.; Xie, J.; Zhang, J.; Hase, W. L. The $F^- + CH_3I \rightarrow FCH_3 + I^-$ Entrance Channel Potential Energy Surface. Comparison of Electronic Structure Methods. *Int. J. Mass Spectrom.* **2014**, DOI: 10.1016/j.ijms.2014.04.006.
(38) Hase, W. L. On the Relationship between Unimolecular Lifetimes and Relative Translational Energy Distributions. *Chem. Phys. Lett.* **1979**, *67*, 263−266.
(39) Townsend, D.; Lahankar, S. A.; Lee, S. K.; Chambreau, S. D.; Suits, A. G.; Zhang, X.; Rheinecker, J.; Harding, L. B.; Bowman, J. M. The Roaming Atom: Straying from the Reaction Path in Formaldehyde Decomposition. *Science* **2004**, *306*, 1158−1161.
(40) Bowman, J. M.; Shepler, B. C. Roaming Radical. *Annu. Rev. Phys. Chem.* **2011**, *62*, 531−553.
(41) Bowman, J. M. Roaming. *Mol. Phys.* **2014**, DOI: 10.1080/00268976.2014.897395.
(42) Thomsen, D. L.; Reece, J. N.; Nichols, C. M.; Hammerum, S.; Bierbaum, V. M. Investigating the *α*-Effect in Gas-Phase S_N2 Reactions of Microsolvated Anions. *J. Am. Chem. Soc.* **2013**, *135*, 15508−15514.
(43) Ceotto, M.; Zhunag, Y.; Hase, W. L. Accelerated Direct Semiclassical Molecular Dynamics Using a Compact Finite Difference Hessian Scheme. *J. Chem. Phys.* **2013**, *9*, 54−64.
(44) Szabó, I.; Császár, A. G.; Czakó, G. Dynamics of the $F^- + CH_3Cl \rightarrow Cl^- + CH_3F$ S_N2 Reaction on a Chemically Accurate Potential Energy Surface. *Chem. Sci.* **2013**, *4*, 4362−4370.